Vibrational excitation in CO_2 via the 3.8-eV resonance*

M. J. W. Boness† and G. J. Schulz
Department of Engineering and Applied Science, Mason Laboratory, Yale University, New Haven, Connecticut 06520
(Received 9 January 1974)

The vibrational excitation by electron impact on CO_2 has been studied in the energy range 3–5 eV by observing scattered electrons at an angle of 90°. Such scattering is dominated by the $^2\Pi_u$ shape resonance. The energy-loss spectrum at 3.6 eV consists of about 30 peaks, which we associate with two progressions of vibrational excitation of the CO_2 molecule, namely, the $n00$ and $n10$ modes. This assignment is consistent with previously measured angular distributions of the inelastically scattered electrons. The energy dependence of the vibrational cross sections exhibits structure. The peaks and valleys of this structure shift to higher energies as the vibrational quantum number of the final state increases. The experimental observations are qualitatively consistent with an extension of the boomerang model which has been developed by Herzenberg for the compound state in N_2.

I. INTRODUCTION

Vibrational excitation of homonuclear diatomic molecules by electron impact at low energies is known to proceed predominantly via shape resonances. A comprehensive bibliography of this subject is contained in a recent review article dealing with the subject of resonances in diatomic molecules.[1] The subject has been extensively studied and the agreement between the experimental and theoretical work[2-4] indicates that the process is now well understood.

A. Vibrational excitation via shape resonances in diatomic molecules

Before proceeding to discuss resonance vibrational excitation of the CO_2 molecule by electron impact, a summary of the characteristic features for the analogous process in diatomic molecules is presented. This will provide a convenient framework for comparison when an attempt is made to interpret and classify the features exhibited by the CO_2 vibrational cross-section data.

Measurements of the energy dependence of vibrational excitation by electron impact have been performed in many diatomic species and they have revealed a considerable variety of features.[1] Broadly speaking the features displayed by the vibrational excitation cross sections depend upon the lifetime of the shape resonance or temporary negative ion which is involved in the reaction.

When the lifetime of the shape resonance is smaller than a typical vibration time, the various vibrational cross sections exhibit a broad featureless hump. A further feature of these short-lived compound states is the rapidly diminishing ratio of the magnitudes of the vibrational excitation cross sections to successive vibrational levels. Such resonances represent the short-lifetime limit of compound states, generally described as the *impulse limit*[3] beyond which the resonance and direct processes are indistinguishable. The 3- to 4-eV shape resonance in hydrogen offers[5,6] an example of this class of resonance.

When the lifetime of the compound state becomes comparable to typical vibrational times, the vibrational cross sections develop an oscillatory structure. The location of the peaks and valleys comprising these oscillations shift toward higher energies as the vibrational quantum number of the final state is increased. This behavior is demonstrated by the first shape resonances in N_2 and CO, located around 2.3 and 1.7 eV, respectively,[5] which possess lifetimes of the order 10^{-14} sec. The behavior of these vibrational cross sections in the case of the 2.3-eV nitrogen resonance have been successfully explained by the boomerang model proposed by Herzenberg,[7] which we discuss and extend in Sec. IV.

As the resonance lifetime increases further, it becomes much larger than the vibration time of the compound state. Under these conditions, the energy dependence of the vibrational cross sections exhibit very narrow, isolated spikes. These spikes remain at constant energy for all final vibrational states and these energies correspond to the vibrational levels of the resonances. An example is the compound state in O_2 in the region 0 to 1 eV.[8,9]

The angular distributions of the resonantly scattered electrons are determined by the partial wave or mixture of partial waves in which the resonance scattering occurs. This information assists in identifying the symmetry of the resonance state. However, in molecules for which

the lifetime of the compound state is comparable or exceeds the rotational period, the angular distribution becomes more nearly isotropic and does not provide us with new information on symmetries.

B. Shape resonances in triatomic molecules

Our knowledge of resonances in triatomic molecules is much less extensive. For an exploration of resonances in triatomic molecules, electron-transmission spectroscopy has been successful in revealing structure in the low-energy total scattering cross section for several triatomic systems.[10,11] This structure has been interpreted as evidence for shape resonances. In CO_2 and NO_2, a series of narrow structures are observed which are identified as vibrational progressions of the compound state. A broad and featureless structure attributable to a shape resonance has been observed in N_2O. Thus, the shape resonance in N_2O appears to have a shorter lifetime compared to the low-lying shape resonances in CO_2 and NO_2.

In the case of CO_2, electron-transmission experiments show a spacing of the structure in the total cross section of approximately 130 meV.[10,11] Similarly spaced structure has been observed by Burrow and Sanche[12] in the differential elastic scattering cross section at a scattering angle of 180°. This structure, which extends from 3 to 5 eV has been attributed to the symmetric-stretch vibrational mode of the resonance. Burrow and Sanche estimated the mean autoionization width of the resonance to lie within the limits 0.13–0.26 eV. Claydon *et al.*[13] have calculated potential-energy curves for the CO_2^- system and their results indicate that the resonance at 3.8 eV is initially a linear configuration of CO_2^-, possessing $^2\Pi_u$ symmetry.

The initial work of Boness and Schulz[14] indicated that the resonance process populates only certain vibrational modes. The experiments of Danner[15] yielded higher-resolution studies of the excitation functions for various vibrational modes as well as angular distributions for many of the energy-loss processes. The angular-distribution measurements have since been successfully interpreted by Andrick and Read,[16] who also confirm that the resonance process should lead only to the excitation of certain modes.

Andrick *et al.*[17] have reported studies of direct vibrational excitation in CO_2 over the energy range 0.5–20 eV. They find strong forward scattering for the optically active modes 001 (asymmetric stretch) and 010 (bending). The optically inactive 100 mode (symmetric stretch) exhibits much lower intensity in forward scattering and the angular distribution of electrons is almost isotropic in the energy range excluding the resonance. The pronounced forward scattering for the optically active modes was interpreted in terms of a dipole interaction resulting from the transition dipole moments associated with these modes. This has been confirmed by Itikawa[18] who has compared the experimental data with the Born approximation. The excitation of the 100 optically inactive mode is attributed by Itikawa to the polarization interaction.

This paper presents new data describing resonance vibrational excitation in CO_2 in the 3- to 5-eV region. We present both energy-loss spectra and the energy dependence of the vibrational cross sections. We find that our interpretation of the energy-loss spectrum is consistent with other experimental evidence available. We also present, qualitatively, a two-dimensional extension of the "boomerang" model, originally developed by Herzenberg[7] for the one-dimensional case of N_2. This boomerang model explains several features of the experiment and it provides us with a graphic insight into the physical mechanisms involved.

II. APPARATUS

A schematic diagram of the electron spectrometer is shown in Fig. 1. A rotatable hemispherical electrostatic analyzer is used to produce a mono-

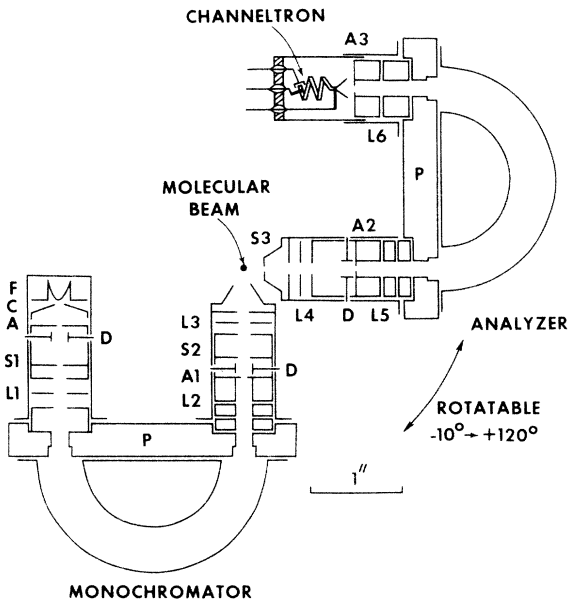

FIG. 1. Schematic diagram of the double hemispherical electron spectrometer. Lenses are designated by L, angular stops by S, imaging apertures by A, deflector plates by D, and mounting plates by P.

energetic beam of electrons which is crossed with a collimated molecular beam. The energy dependence of the scattered electrons is analyzed by means of a second identical hemispherical selector. The instrument uses virtual slits similar to those employed by Simpson.[19] Since this instrument has not been described previously, we give a rather detailed exposition below.

Imaging and energy control of the electron beam are performed by a number of lenses $L1-L6$. Two basic lens types are employed, namely, the three-aperture variable-ratio lens, which has been analyzed by Read[20] and a novel combination of tube lenses, $L2$ and $L5$, whose separate characteristics are due to Spangenberg.[21] By means of an external switching circuit these tube lenses may be operated with any one of three fixed voltage ratios, 0.1, 1, and 10. This flexibility is achieved by constructing the lens from four cylindrical elements of equal diameter, one element being plate P. The two inner elements are each half the length of the outer elements. Connecting the center elements together and the outer elements together transforms the system to a symmetric three-cylinder einzel lens with a voltage ratio of unity. Connecting the first element to the second and the third element to the fourth produces a symmetric two-cylinder lens. Application of the appropriate potentials to this two-cylinder lens permits either of the voltage ratios 0.1 or 10 to be selected.

Electrons emitted from the thoria-coated iridium hairpin filament F, pass through a 1.3-mm-diam hole in the Pierce cathode[22] C and emerge from the 0.6-mm aperture in the anode A. The gun is operated under space-charge limited conditions with an anode potential of 25 V. The zoom lens $L1$ images the anode aperture in the entrance plane of the monochromator with approximately unity magnification, thus forming a virtual entrance aperture, and it also decelerates the beam to the required energy, typically 1.5–2.5 eV. Electrode $S1$ serves as the angular stop for the injection optics and limits the half-angle of the beam at the monochromator to approximately 0.07 rad. The radii of the inner and outer hemispheres comprising the monochromator are 1.9 and 3.2 cm, respectively. They are concentrically located on the mounting plate P and insulated from it using sapphire balls of 1.5-mm diameter. In order to compensate for the fringing fields at the entrance and exit apertures of the monochromator and analyzer, the Herzog correction[23] is applied. Our particular dimensions require the mounting plates P to be located 2.7 mm from the end of the hemispheres and to contain apertures of 6.3-mm diameter. The spectrum of electron energies dispersed in the focal plane of the monochromator is imaged by the cylinder lens $L2$ onto the aperture $A1$ (0.75-mm diameter), which transmits a portion of the distribution. The zoom lens $L3$ forms an image of aperture $A1$ in the collision region and controls the impact energy of the colliding electron beam. $S2$ is the angular stop for the monochromator exit optics.

The electron beam crosses the molecular beam which is formed by allowing gas to effuse from a small tube of 0.75-mm diameter. A cone of scattered electrons of half-angle 0.07 rad defined by the angular stop $S3$ (0.5-mm diameter) is transmitted to the analyzer at the required energy by a similar combination of tube and aperture lenses $L4$ and $L5$. The exit focal plane of the analyzer is imaged onto the aperture $A3$ (0.75-mm diameter) by the einzel cylinder lens $L6$. Finally the electrons are detected by a channeltron multiplier.

Small perturbations of the beam arising from stray fields are compensated by applying small potentials to the various perpendicular pairs of deflection plates D, placed at intervals along the beam trajectory. Magnetic fields are screened by a double layer of magnetic shields. The residual field close to the experimental region measured with a gaussmeter does not exceed 10 mG.

All parts of the spectrometer were constructed from molybdenum and machined to a high-quality polish. Prior to assembly all components were placed in an ultrasonic cleaner, washed with acetone, and finally dried after rinsing in distilled water. Facility for baking the system to 350° exists. However after operating for one year in gases such as CO, CO_2, and H_2, it has not yet been found necessary to employ this procedure.

The spectrometer is contained within a stainless-steel vacuum chamber which is evacuated by a high-speed 6-in. oil diffusion pump connected to a liquid-nitrogen trap. The base pressure of the system is 2×10^{-8} torr. With the molecular beam in operation, the pressure rises to 2×10^{-5} torr.

Operating the monochromator to pass electrons of 1.6-eV energy yields a primary-beam intensity of 2×10^{-9} A. The full width at half-maximum (FWHM) of the elastically scattered electron distribution obtained when operating the analyzer also at 1.6 eV is 45 meV. Assuming identical Gaussian transmission functions for both selectors, this indicates a resolution (FWHM) of 30 meV for the primary beam. Alternatively the resolution may be determined by examining the widths of narrow resonances in both the elastic and inelastic scattering cross sections. Agreement between the results derived from these separate techniques demonstrates the absence of potential variations within the collision volume.

Pulses from the channeltron multiplier are

first decoupled from the high voltage (2800 V) existing at the output of the channeltron by a 0.002-μF capacitor and the pulses are then applied to the input of an integrated-circuit field-effect transistor (FET) preamplifier. The output pulses are further amplified, shaped, and amplitude limited by a single-channel analyzer. The counting rate is displayed on a scaler and a rate meter. For sufficiently high counting rates the analog output of the rate meter is displayed on the X-Y plotter. Low counting rates are measured by a variety of signal-averaging techniques provided by an on-line PDP-11 computer. The scanning voltages appropriate to the particular mode of operation of the instrument (inelastic or elastic) are supplied by a high-precision (±1 meV) digitally programable power supply interfaced to a PDP-11 computer which programs the supply in response to instructions typed on a teletype terminal. This scanning voltage is either synchronized with the computer channel address or applied to the X axis of the X-Y plotter depending on the particular mode of data acquisition employed. Data retrieval from the computer memory is accomplished in the form of a point plot of channel contents as a function of channel location directly on the X-Y plotter. The channel contents may also be printed out by the teletype.

III. RESULTS

A. Energy-loss spectrum

Figure 2 shows an energy-loss spectrum obtained at an incident energy of 3.65 eV and a scattering angle of 90°. This spectrum was recorded by holding constant the incident energy and using the second 180° selector to analyze the energy distribution of the scattered electrons. The energy of the incident beam was calibrated by mixing N_2 into the CO_2 molecular beam and measuring the position of the first peak in the excitation function to the first vibrational level, $v=1$ in N_2. The position of this peak has previously been determined as 2.0 eV.[5] The multiplication factors for the four separate sections of the spectrum are, from left to right, ×1, ×10, ×40, and ×100. However, the attenuation in amplitude of the spectrum towards higher-energy losses is strongly influenced by various instrumental factors so that the ratio of amplitudes of different peaks do not correspond to the true ratio of the absolute magnitudes of the cross sections. The instrumental effects tend to suppress the amplitudes of the higher-energy-loss peaks when the sweep extends over as large a range as shown in Fig. 2. The *proper* ratio of peak heights can be obtained by maximizing separately *each peak* of the energy-loss spectrum of Fig. 2 or by choosing a more limited range of the energy-loss spectrum. Indicated (top of Fig. 2) are the calculated positions of the bending mode, $0n0$, the symmetric-stretch mode, $n00$, and the symmetric-stretch mode plus one quantum of bending, $n10$.

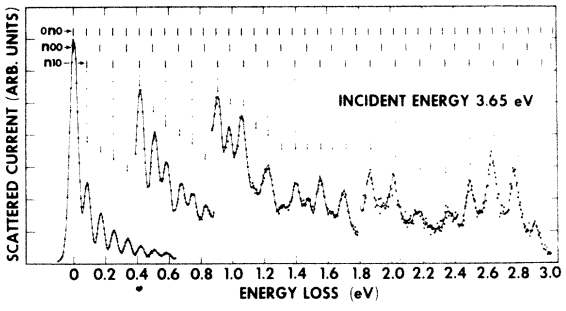

FIG. 2. Energy-loss spectrum obtained at an angle of observation of 90° and an incident energy of 3.65 eV. On top of the figure we indicate the calculated positions for the vibrational progressions $0n0$, $n00$, and $n10$. The observed spectrum is interpreted in terms of two series, namely, $n00$ and $n10$. See the text.

The identification of the various energy-loss peaks of Fig. 2 cannot be unambiguously established from peak location alone, since overlapping combination modes exist, in addition to the modes indicated on Fig. 2. However, another feature of the spectrum does offer assistance in this respect. An over-all view of the spectrum suggests that two separate series are present. The first possesses an energy-separation characteristic of the symmetric-stretch mode. This series gradually diminishes in amplitude towards higher-energy losses and cannot be detected beyond an energy loss of 1.6 eV. The other series possesses the same separation but it is separated from the first series by about 80 mV and it persists with an oscillating envelope amplitude to the end of the spectrum. Thus, the peak spacing in the first half of the spectrum is one-half the spacing in the second half. Extrapolating back towards the elastic peak from high-energy losses identifies 010 as the first number of the longer series and the 0.170-eV peak as the first member of the shorter series. The *simplest* designation of the two series consistent with these observations is $n10$ for the longer series and $n00$ for the shorter series. Members of the two series are identified by dotted ($n00$) and dashed ($n10$) lines originating at the calculated locations of the respective vibrational energy levels.

B. Energy dependence

Figure 3 presents excitation functions for five arbitrary peaks in the energy-loss spectrum. These data were recorded by adjusting the analyzer to accept only those electrons having lost a specific amount of energy, appropriate to the loss process of interest. The incident energy is then scanned over the range of interest, thus producing the excitation function shown in Fig. 3. Excitation functions corresponding to energy losses of 0.083, 0.505, 1.060, 2.010, and 2.900 eV were recorded. The preceding interpretation of the energy-loss spectrum leads to the identification of these levels as (010), (300), (610), (12,1,0), and (18,1,0), respectively. Oscillations appear in each of the excitation functions. The spacing of the structure in the 010 excitation function agrees exactly with the value of 131 meV measured by Danner.[15] This value also agrees closely with the values obtained from transmission studies[10,11] and from the study of elastic scattering at 180°.[12] Since the spacing of the structure for higher-energy losses is much larger, the agreement in the spacing of the structure obtained in transmission experiments, on the one hand, and the elastic and 010 cross sections on the other, illustrates that the total cross section is dominated by the contribution from the elastic and low-lying vibrational cross sections.

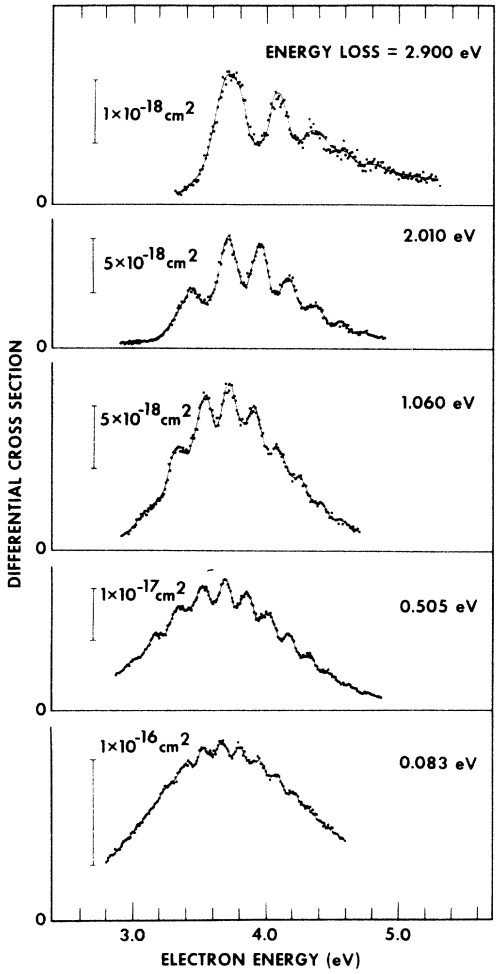

FIG. 3. Energy dependence of the differential cross sections for five different energy-loss processes. The magnitude of the differential cross sections are shown by the vertical bars. Note that the positions of the peaks shift on the energy scale.

C. Shifting peaks

The positions of the peaks in the vibrational cross sections shift towards higher energies as a function of the magnitude of the energy loss. This is illustrated in Fig. 4 in which we plot peak position as a function of energy loss. Straight lines are drawn through points identifying the location of corresponding peaks in the different vibrational cross sections, that is 1st peak, 2nd peak, and so on. The peak number is indicated on the right of the diagram. In the case of the long-lifetime limit of the compound state, the lines would be

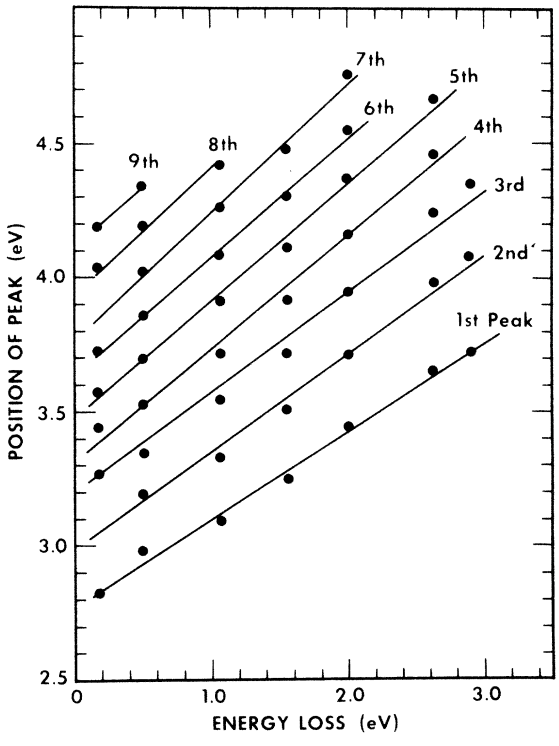

FIG. 4. Positions of the peaks plotted against energy loss. The energies of the peaks shift to higher energies as the energy loss increases. This shift is similar to the case of N_2 and it indicates that the resonance has an intermediate lifetime.

horizontal, indicating stationary peaks in the various vibrational cross sections. Data abstracted from other measured vibrational cross sections now shown in Fig. 3 have also been included in the compilation of Fig. 4.

D. Magnitude of the cross sections

An incomplete knowledge of many instrumental parameters precludes any attempt to make absolute cross-section measurements in the present experiment. Usually we normalize our measured cross sections to the theoretical values for the differential elastic scattering cross section in helium calculated by Labahn and Callaway.[24] However, in the case of CO_2, various reliable absolute measurements for both elastic and inelastic cross sections exist[14,15,25,26] and, therefore, we have chosen to normalize directly to the corresponding cross sections obtained by Danner.[15] Since we prefer to present total cross-section data, care must be taken to take account of variations in the angular distributions. As we shall discuss fully in Sec. IV, differences in angular distributions do exist for the various energy-loss processes and for this reason, it is necessary to separately normalize the cross sections for 010, the first member of the short series 100, and the second member of the long series 110 (which exhibits a different angular dependence from the first member 010). On this basis we are then able to obtain the cross sections for various higher-energy-loss modes by measuring the relative magnitudes of the vibrational cross sections similar to and including those presented in Fig. 3. These data are plotted in Fig. 5. For comparison we have included the work of Danner,[15] Lowke *et al.*,[26] and Spence, Mauer, and Schulz.[25] The latter authors employed the trapped-electron technique and, therefore, did not measure separately the cross sections for the various discrete loss processes. Instead their measurement represents a summation of total cross sections at 3.8 eV beginning with the most highly excited mode possible (total energy loss) and then successively including the cross section to less and less highly excited modes, eventually obtaining the total cross section at 3.8 eV summed over all possible loss processes. In their paper this functional dependence of the integrated cross sections at 3.8 eV is represented in terms of the "well depth W."

Finally in Table I we have listed our calculated values of the vibrational energy levels corresponding to the $n00$ and $n10$ modes. These were calculated according to the formula and fundamental spectroscopic constants given by Herzberg[27] together with the values for the anharmonic coefficients determined by Courtoy.[28] Adjacent to the values of these calculated energy levels we have listed the measured position of the energy-loss peak obtained from data such as shown in Fig. 2. Peak positions listed beyond the range of the energy-loss spectrum shown in Fig. 2 were obtained from separate spectra measured at slightly different incident energies.

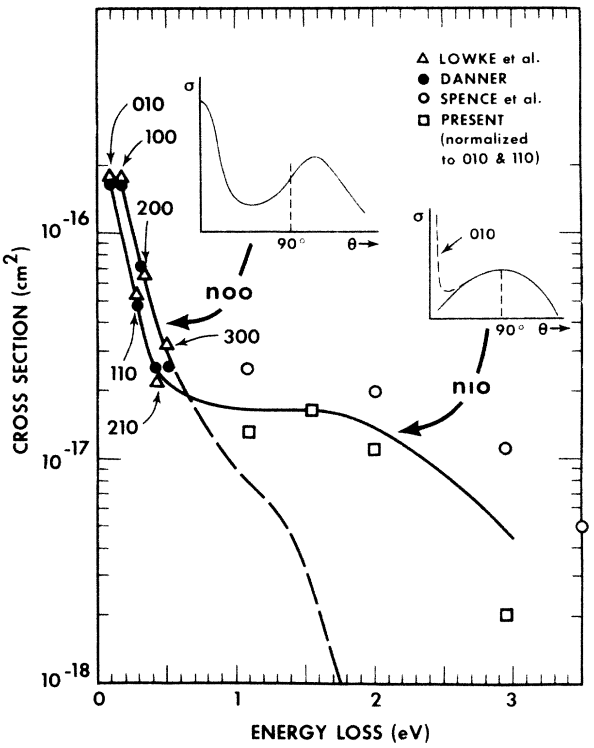

FIG. 5. Magnitude of vibrational cross sections vs energy loss. Shown, in addition to the present data, are those of Lowke *et al.* (Ref. 26), Danner (Ref. 15), and Spence *et al.* (Ref. 25). The heavy lines connect points belonging to two series, $n10$ and $n00$. The dashed portion of the curve for the $n00$ series (0.6–1.7 eV) is based on present data, but this portion is afflicted with a large error. The angular distributions of these two series are different. The angular distributions measured by Danner (Ref. 15) are sketched in. The angular distribution for the 010 mode is unique and is shown dashed.

IV. INTERPRETATION

The vibrational cross sections presented in Fig. 3 are reminiscent of the vibrational cross sections exhibited by N_2 in the vicinity of the 2.3-eV N_2^- shape resonance.[5] In each case, the energy dependence shows an oscillatory behavior. The peaks of these oscillations shift to higher energies and the separation between the peaks increases as a function of the energy of the final vibrational level (see Fig. 4). These features in N_2^- have

TABLE I. Vibrational energy levels in CO_2.

Calculated energy level (eV)			Experimental position of energy-loss peak (eV)
Designation	$n10$	$n00$	Error ± 0.01 eV
01^10	0.083		0.083
10^00		0.167	0.168
11^10	0.250		0.250
20^00		0.333	0.335
21^10	0.416		0.415
30^00		0.498	0.500
310	0.582		0.580
400		0.662	0.665
410	0.746		0.740
500		0.825	0.820
510	0.910		0.900
600		0.987	0.985
610	1.072		1.06
700		1.149	1.14
710	1.234		1.23
800		1.309	1.30
810	1.395		1.39
900		1.469	1.47
910	1.555		1.55
10,00		1.627	1.61
10,10	1.714		1.70
11,00		1.785	
11,10	1.872		1.87
12,00		1.942	
12,10	2.030		2.02
13,00		2.098	
13,10	2.186		2.17
14,00		2.253	
14,10	2.342		2.35
15,00		2.407	
15,10	2.496		2.50
16,00		2.561	
16,10	2.650		2.65
17,00		2.713	
17,10	2.803		2.78
18,00		2.864	
18,10	2.955		2.93
19,00		3.015	
19,10	3.106		3.10
20,00		3.165	
20,10	3.256		3.23
21,00		3.313	
21,10	3.405		

been interpreted in terms of a compound state of intermediate lifetime.[7] It is suggested that an analogous situation prevails in the case of the CO_2 resonance near 3.8 eV and it can be expected that an extension of the theoretical model which is valid for N_2^- should be applicable to CO_2^-.

In Sec. I reference was made to the boomerang model which successfully explained the behavior of the vibrational cross sections in nitrogen in the vicinity of the 2.3-eV shape resonance.[4] In order to interpret both the energy-loss spectrum and the behavior of the vibrational cross sections in CO_2, we present below a model which is based on Herzenberg's boomerang concept. It is appropriate at this point to review the more significant aspects of this model which will be germane to our interpretation of the CO_2^- 3.8-eV resonance.

A. Boomerang model in one dimension

Herzenberg proposed that once the electron attaches to the N_2 molecule the nuclear wave function propagates across the N_2^- potential well in such a manner that only one reflection of the wave packet is permitted. The wave packet is completely annihilated by autoionization when it reaches the end of the first cycle. Thus only a single outgoing and a single reflected wave are considered. This process is indicated schematically in Fig. 6. The superposition of these two waves produces a standing wave whose nodes drift slowly in position as a function of electron energy. Calculation of the overlap integral between this standing wave and the vibrational states of the neutral molecule reveals that the energy dependences of the vibrational cross sections oscillate and that the peaks occur at different energies depending on the final channels of excitation. A certain functional dependence of the autoionization width $\Gamma(R)$ on internuclear separation R, has to be assumed, governed by the relative locations of the N_2 and N_2^- potential-energy curves. The variation of $\Gamma(R)$ is schematically indicated at the bottom of Fig. 6. Finally, in order to reproduce qualitative agreement with the experimental data, the magnitude of $\Gamma(R)$ has

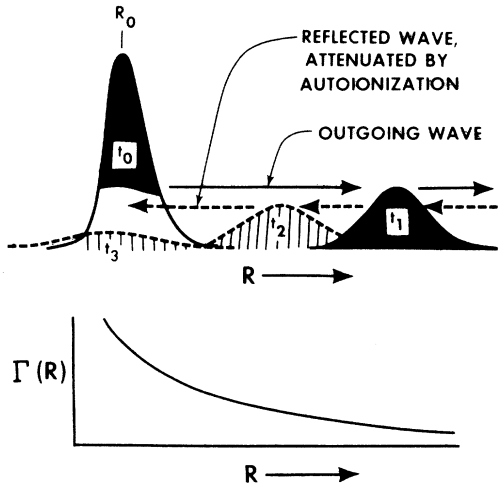

FIG. 6. Schematic diagram for the boomerang model in one dimension, showing the time evolution of the nuclear wave function. Below we show that the autoionization width of the resonance is a function of internuclear separation. The model has been developed by Herzenberg (Ref. 7).

to be adjusted to provide the desired annihilation rate for the nuclear wave function. An essential feature of this model is the interference between the outgoing and reflected nuclear wave function, without which it is impossible to reproduce the oscillatory energy dependence of the cross sections combined with a shift in the peaks.

B. Boomerang model in two dimensions

Propagation of the nuclear wave function within the potential well of the N_2^- ion is adequately described in terms of a single coordinate, namely, the internuclear separation. Application of the boomerang model to a triatomic molecule is complicated by the increased number of normal nuclear modes. Linear triatomic systems, in general, possess four normal nuclear modes, symmetric stretch, antisymmetric stretch, and two bending modes, the latter being degenerate. The symmetry of the model excludes asymmetric deformation via the compound state.[16] Two coordinates are, therefore, eliminated which permits the propagation of the nuclear wave function to be expressed as a function of the remaining *two coordinates*, symmetric stretch and bending.

The variation of the potential energy for the lowest shape resonance in CO_2, $^2\Pi_u$, as a function of the symmetric stretch and bending coordinates have been calculated by Claydon *et al.*[13] and their results are reproduced in Figs. 7(a) and 7(b), respectively. Fig. 7(b) indicates that departure of the CO_2^- ion from a linear configuration produces a splitting of the degenerate $^2\Pi_u$ configuration into the $^2A_1$ and $^2B_1$ components. In each figure the variation of potential energy is calculated assuming that the remaining coordinates retain their equilibrium configurations appropriate to CO_2. Thus, in Fig. 7(a), the bond angle is 180° and in Fig. 7(b), the symmetric-stretch equilibrium bond length is 1.23 Å.

Consider now the propagation of the nuclear wave function with respect to the two coordinates. At the instant of electron attachment the derivative of potential energy with respect to the symmetric-stretch coordinate in the CO_2^- potential curve is negative and the nuclei immediately roll down into the valley shown in Fig. 7(a). However, for bending, the derivative is zero at 180° where attachment occurs and the nuclei are in a situation of unstable equilibrium. Due to the thermal or zero-point vibrational motion, however, the equilibrium is disturbed and the nuclei *very slowly* roll down the valley of the $^2A_1$ curve or up the sides of the valley of the $^2B_1$ curve shown in Fig. 7(b). In short, the negative ion attempts to reach its equilibrium configuration by bending very slowly but moving along the symmetric-stretch coordinate relatively rapidly. This proposition has previously been advanced by Taylor.[29]

Fig. 8 represents schematically the propagation of the envelope of the nuclear wave packet as a function of the symmetric stretch and bending coordinates in the potential well of the negative ion. The diagram has been constructed as an extension of the boomerang model, by assuming that only one reflection of the wave packet occurs along the symmetric-stretch direction, after which the wave packet is annihilated by autoionization. Accompanying the excursion in the symmetric-stretch direction is a *small* excursion in the bending direction. The smallness of the bending excursion is a result of the anharmonic nature of the variation of the potential energy in

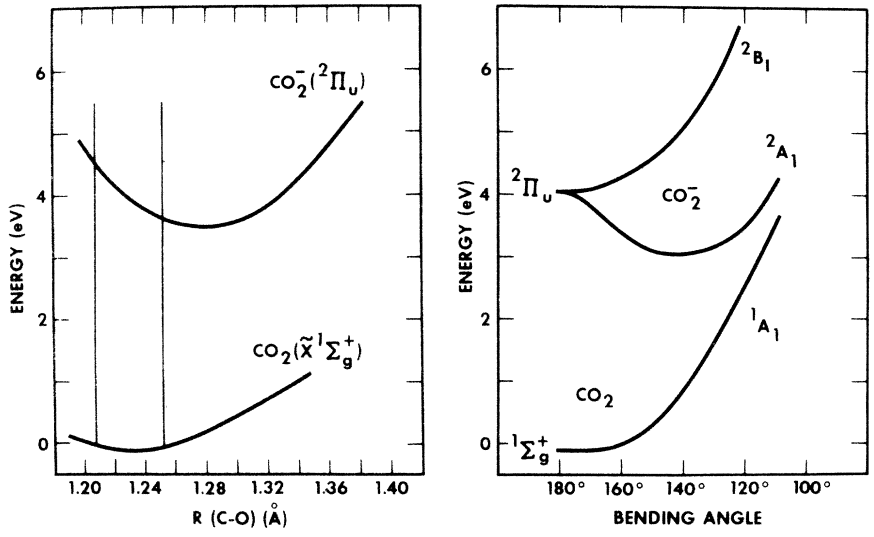

FIG. 7. Potential-energy variation for the $^2\Pi_u$ resonance of CO_2 vs symmetric stretch and bending coordinates. From Claydon, Segal, and Taylor (Ref. 13).

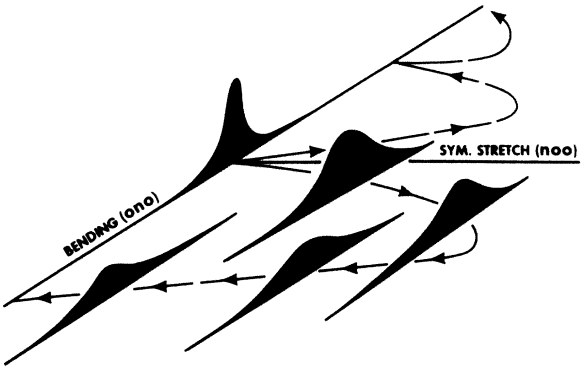

FIG. 8. Schematic diagram for the boomerang model in two dimensions, applicable to the case of CO_2. The nuclear wave function performs a single full excursion in the symmetric-stretch direction and a small excursion in the bending direction.

the bending direction. Since the bending excursion is much less than one complete cycle, no interference occurs along this coordinate and all the interference structure occurring in the energy dependence of the cross section (Fig. 3) is a consequence of the interference along the symmetric-stretch coordinate. Upper and lower dashed trajectories are drawn corresponding to the two possible directions for deformation of the bond angle from 180°. Two loops have been included in the upper trajectory. The second loop corresponds to two additional reflections of the nuclear wave packet and has been included to indicate the development of the trajectory if additional oscillations occur along the symmetric-stretch coordinate. Commencing at the intersection of the axes and proceeding in the direction of the arrows, the time evolution of the envelope of the wave packet is indicated at a number of points along the lower trajectory. At the expense of completeness but in the interests of clarity, only sections through the wave packet parallel to the bending coordinate are shown.

C. Decay of the two-dimensional boomerang

The discussion above implies that the Franck-Condon overlap between the negative-ion state and the neutral ground state along the symmetric-stretch coordinate encompasses many highly excited symmetric-stretch vibrational levels of the neutral ground state. However, since only a small deformation of the bend angle occurs during the lifetime of the resonance, the bending coordinate overlap includes very few bending vibrational levels. Thus, copious symmetric-stretch excitation should occur accompanied by little or no bending excitation. These conclusions are in keeping with our interpretation of the energy-loss spectrum.

We now have to ask why the (n10) series persists longer than the pure symmetric-stretch series (n00). This is best understood in terms of the time evolution of the negative-ion nuclear wave function shown in Fig. 8.

At early times, the wave packet propagates from the intersection of the axes along the dotted trajectory. Early autoionization events occur with small to intermediate excursions along the symmetric-stretch coordinate and pratically no bending excursion. By considering the Franck-Condon overlap, autoionization events at these early times populate low to intermediate levels of the pure symmetric-stretch system. Decay at later times populates the higher symmetric-stretch levels and gradually a bending quantum is included. At the turning point of the symmetric-stretch trajectory the highest accessible symmetric-stretch modes, in addition to the first bending level, are excited. After reflection of the wave packet, progressively lower-lying symmetric-stretch modes are excited, always accompanied by one bending quantum. The ratio of the length of the two series in the energy-loss spectrum indicates that significant excitation of the bending mode occurs after approximately one quarter of the trajectory has been traversed.

Autoionization continuously diminishes the amplitude of the propagating wave packet, but this does not imply that the vibrational levels being populated will exhibit progressively diminishing cross sections since the relative magnitude of the cross sections depends also upon the overlap integral between the negative-ion state and the vibrational levels of the neutral molecule. In order to evaluate this overlap integral, the time-independent picture for the process must be considered, i.e., the wave function required for the negative-ion state corresponds to the standing wave generated by the outgoing and reflected waves.[4]

D. Relationship to angular distributions

Inspection of the angular-distribution measurements of Danner[15] lends support to the model advanced above. Danner measured angular distributions for those electrons having lost energies equal to 0.083, 0.167, 0.255, 0.339, 0.422, 0.505, and 0.591 eV at impact energies within the domain of the resonance. These loss processes correspond to the first seven peaks of the energy-loss spectrum of Fig. 2. Their measurements revealed two distinct types of angular distributions and *alternate* energy-loss processes exhibited identical distributions. The angular distribution of elec-

trons having excited the 010 bending mode possessed an anomalous feature not exhibited by the other members of the same series, namely, a sharp peak in the forward direction. This peak arises from the direct interaction which couples via the transition dipole moment and which is unimportant for the higher-loss processes.[18]

The angular distributions observed by Danner are sketched in Fig. 5. The arrows indicate which series each distribution characterizes. The direct component of the 010 loss process is indicated by the dashed portion of the $n10$ distribution.

Andrick and Read[16] derived expressions for the angular distributions of electrons resonantly scattered by molecules and demonstrated how these distributions depend upon the vibronic symmetries of the molecular states. By adjusting the amplitudes and phases of the partial waves contributing to the particular excitation process they were able to obtain excellent least-squares fits to the experimental data obtained for the 0.083- and 0.172-eV loss processes. The partial-wave composition was deduced from symmetry considerations assuming that the loss processes corresponded to excitation of the 010 and 100 modes, respectively. Energetically, the excitation of the 100 mode could not be resolved from the 020 mode, however, the excellence of the fit to the experimental angular distributions resolves this ambiguity and confirms the identification of the loss process as 100, which is in agreement with our interpretation.

The postulate that the two series $n10$ and $n00$ are excited is also consistent with the angular-distribution measurements. The series possess different vibronic symmetries which are constant within a particular series. The theoretically predicted distributions conform to the experimental measurements. Each member of a bending series, such as $0n0$, would possess different vibronic symmetry and therefore produce different angular distributions. The angular-distribution measurements thus offer strong support to the contention that higher bending modes are not excited since only two types of distribution are observed.

V. CONCLUSIONS

The study of electron scattering at 90° in carbon dioxide presents a particularly suitable system for the aim of our present work: To extend the understanding of shape resonances gained from diatomic molecules to triatomic systems. The linear, symmetric structure of CO_2 in the ground electronic state enables us to discard the asymmetric-stretch mode from our consideration, thus leaving only the bending and symmetric-stretch modes to be considered. The energy-loss spectra substantiate this hypothesis and we find that only two progressions of final vibrational states are excited via the shape resonance, namely, the $n00$ and $n10$ modes. The energy dependence of the vibrational cross sections shows peaks and valleys which shift to higher energies as the vibrational quantum number increases. From an analogy with the case of N_2, we argue that the boomerang model developed for N_2 should be applicable, in slightly modified form, to CO_2 as well. This places the lifetime of the $^2\Pi_u$ resonance in the range of 10^{-14} sec. The lifetime is long enough for the nuclear wave function to perform one complete cycle in the symmetric-stretch direction, but only a fraction of a cycle in the bending direction.

It should be noted that we have chosen an angle of observation (90°) which is particularly favorable for the measurement of resonance scattering alone. We confidently expect that at other angles of observation additional vibrational modes will appear (e.g., the asymmetric-stretch mode), which result from direct scattering processes.

We can expect that other linear triatomic molecules will have longer or shorter lifetimes. When the lifetime of the resonance is *longer* than in the case of CO_2, we expect higher bending series to be excited, in addition to the $n10$ progression. In such cases we would expect to observe series such as $n20$, $n30$, etc. In the case of asymmetric molecules, we would also expect the excitation of some asymmetric-stretch modes via a shape resonance.

When the lifetime of the resonance is *shorter* than in the case of CO_2, we would expect a smooth energy dependence for the vibrational cross sections. Possibly there may be cases in which the lifetime of the resonance is so short that only the symmetric-stretch mode, without any quanta of bending, would be excited.

ACKNOWLEDGMENTS

We are indebted to A. Herzenberg for frequent discussions, especially in connection with the theory. To Charles Minter of the Yale Computer Science Department go our sincere thanks for developing the software and the hardware which enabled us to make effective use of an on-line computer. We benefited from the advice of P. D. Burrow and S. F. Wong, to whom thanks are due. The competent technical assistance of J. Kearney, R. Downing, W. Sinski, and G. Vogel was essential for the completion of a complex apparatus.

*Work supported by the Office of Naval Research.
†Present address: AVCO-Everett Research Lab, Everett, Mass. 02149.
[1]G. J. Schulz, Rev. Mod. Phys. 45, 423 (1973).
[2]J. N. Bardsley, A. Herzenberg, and F. Mandl, Proc. Phys. Soc. Lond. 89, 321 (1966).
[3]A. Herzenberg and F. Mandl, Proc. R. Soc. Lond. A 270, 48 (1962).
[4]D. T. Birtwistle and A. Herzenberg, J. Phys. B 4, 53 (1971).
[5]G. J. Schulz, Phys. Rev. 135, A988 (1964).
[6]H. Ehrhardt, L. Langhans, F. Linder, and H. S. Taylor, Phys. Rev. 173, 222 (1968).
[7]A. Herzenberg, J. Phys. B 1, 548 (1968).
[8]D. Spence and G. J. Schulz, Phys. Rev. A 2, 1802 (1970).
[9]F. Linder and H. Schmidt, Z. Naturforsch. 26a, 1617 (1971).
[10]M. J. W. Boness, J. B. Hasted, and J. W. Larkin, Proc. R. Soc. Lond. A 305, 493 (1968).
[11]L. Sanche and G. J. Schulz, J. Chem. Phys. 58, 479 (1973).
[12]P. D. Burrow and L. Sanche, Phys. Rev. Lett. 28, 333 (1972).
[13]C. R. Claydon, G. A. Segal, and H. S. Taylor, J. Chem. Phys. 52, 3387 (1970). See also M. Krauss and D. Neumann, Chem. Phys. Lett. 14, 26 (1972).
[14]M. J. W. Boness and G. J. Schulz, Phys. Rev. Lett. 21, 1031 (1968).
[15]D. Danner, thesis (Physikalisches Institut der Universitat Freiberg, Germany, 1970) (unpublished).
[16]D. Andrick and F. H. Read, J. Phys. B 4, 389 (1971).
[17]A. Andrick, D. Danner, and H. Ehrhardt, Phys. Lett. A29, 346 (1969).
[18]Y. Itikawa, Phys. Rev. A 3, 831 (1971).
[19]J. A. Simpson, Rev. Sci. Instrum. 35, 1698 (1964).
[20]F. H. Read, J. Phys. E 3, 127 (1970).
[21]K. Spangenberg, *Vacuum Tubes* (McGraw Hill, New York, 1948).
[22]J. R. Pierce, *Theory and Design of Electron Beams*, 2nd ed. (Van Nostrand, Princeton, N. J., 1954).
[23]R. Herzog, Z. Phys. 47, 596 (1935).
[24]R. W. Labahn and J. Callaway, Phys. Rev. A 2, 366 (1970).
[25]D. Spence, J. L. Mauer, and G. J. Schulz, J. Chem. Phys. 57, 5516 (1972).
[26]J. J. Lowke, A. V. Phelps, and B. W. Irwin, J. Appl. Phys. 4, 4664 (1973).
[27]G. Herzberg, *The Spectra of Polyatomic Molecules* (Van Nostrand, Princeton, N. J. 1966).
[28]C. P. Courtoy, Ann. Soc. Sci. Brux. 1 73, 5 (1959).
[29]H. S. Taylor (private communication).